Accepted Manuscript

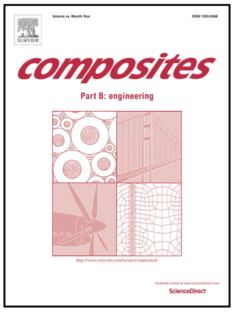

A multiscale XFEM approach to investigate the fracture behavior of bio-inspired composite materials

Andre E. Vellwock, Laura Vergani, Flavia Libonati

PII: S1359-8368(17)33696-X

DOI: 10.1016/j.compositesb.2017.12.062

Reference: JCOMB 5491

To appear in: *Composites Part B*

Received Date: 27 October 2017

Revised Date: 30 December 2017

Accepted Date: 30 December 2017

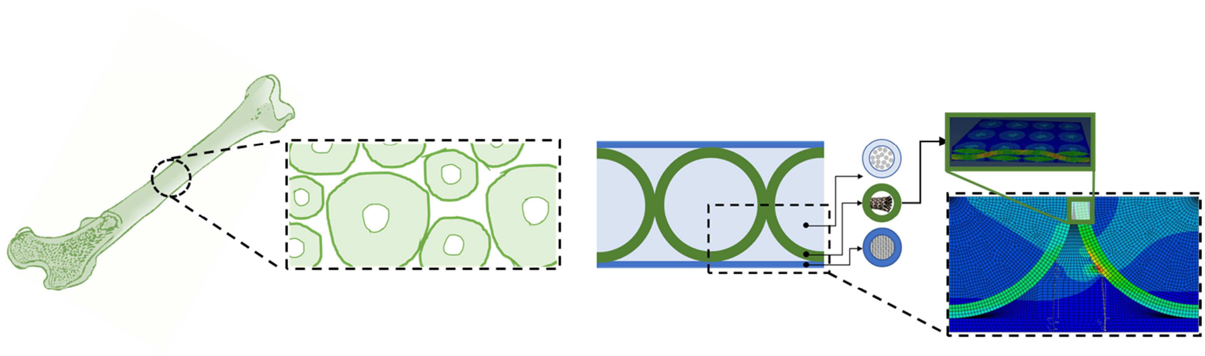

A multiscale XFEM approach to investigate the fracture behavior of bio-inspired composite materials

*Andre E. Vellwock, Laura Vergani, and Flavia Libonati**

Department of Mechanical Engineering, Politecnico di Milano, Milan, Italy

*Corresponding author: *flavia.libonati@polimi.it*

Abstract

In the setting of emerging approaches for material design, we investigate the use of extended finite element method (XFEM) to predict the behavior of a newly designed bone-inspired fiber-reinforced composite and to elucidate the role of the characteristic microstructural features and interfaces on the overall fracture behavior. The outcome of the simulations, showing a good agreement with the experimental results, reveals the fundamental role played by the heterogeneous microstructure in altering the stress field, reducing the stress concentration at the crack tip, and the crucial role of the interface region (*i.e.* cement line) in fostering the activation of characteristic toughening mechanisms, thus increasing the overall flaw tolerance of the composite.

Keywords:

B. Fracture

C. Numerical analysis; Computational modeling;

XFEM (Extended Finite Element Method)

1. Introduction

Optimized for billions of years, many natural materials are considered today models of ideal design, being simultaneously lightweight, stiff, strong and tough. Examples are bone, which provides supports to many animal bodies, nacre and seashells, working as natural body armors and providing protection from external predators' attacks, bamboo, whose gradient structure guarantees an augmented flexural rigidity, enabling protection from crosswind and gravity. Ancient but ever-intriguing, these materials are paradigms of natural structural composites, made of few universal constituents and achieving - through a sophisticated design – a unique combination of mechanical properties, bypassing the trade-off faced by synthetic engineering materials [1]. Traditional structural materials, indeed, continuously face a typical engineering issue of satisfying both strength and toughness requirements. For instance, ceramics provide high strength with a low toughness, whereas steel and metals have high toughness and a limited strength. Composites often represent a good compromise, being lightweight and stiff and offering a good balance with strength-toughness [2]. In particular, fiber-reinforced composites, which present the highest stiffness-to-weight and strength-to-weight ratio, represent an attractive solution for structural applications where the weight is a crucial aspect (e.g. automotive and aerospace) [3–5]. However, they often fail in a brittle way. Enhancing the fracture toughness, by promoting larger energy release before failure, will increase the intrinsic safety of such materials, also fostering their adoption for diverse structural applications.

Drawing inspiration from nature can offer a path towards enhancing their resistance to fracture. Bone, in particular, may represent an excellent biomimetic model for novel composite design. Bone is a lightweight strong and tough natural composite made of hydroxyapatite mineral crystals, providing stiffness and strength, interspersed into an organic matrix (mainly made of collagen) that confers flexibility to the whole tissue. These two building blocks (hydroxyapatite and collagen), arranged into a multiscale hierarchical structure, create a unique composite, whose overall properties far exceed those of the individual components, especially fracture toughness [6]. The enhancement of fracture toughness, occurring in bone, is due to the coexistence of intrinsic and extrinsic mechanisms: the former increase microstructural resistance to crack initiation and growth, whereas the latter act behind the crack tip, reducing the crack-driving force [7]. These mechanisms mainly occur at micro-to-nanoscale and the microstructural organization is thought to play a crucial role in improving toughness, by promoting the activation of such mechanisms. Bone microstructure is generally characterized by repeating cylindrical features, called osteons, made by concentric lamellae and a central vascular canal, aka Haversian c. The outer boundaries of the osteons are surrounded by a sheath, named cement line, which is a weak interface resulting from the remodeling process (**Fig. 1(a)**) and playing an active role in enhancing bone toughness. At this scale, two main toughening mechanisms can be identified: crack bridging and crack deflection/twisting [8,9]. Crack bridging occurs when microcracks form ahead of the propagating crack, inhibiting its progress. Crack deflection/twisting occurs primarily in the transverse direction, where the osteons and the cement line are able to deflect the crack path, increasing the energy dissipation and toughening the material.

The microstructure has also shown to widely affect the mechanical properties of other materials [2,10]. Guan *et al* [11] demonstrated how the fiber network microstructure can alter not only the mechanical properties, but also the failure mechanism of natural composites. Bermejo [12] confirmed the influence of a tailored microarchitecture on the crack path, thus affecting the overall fracture behavior. In composite manufacturing, techniques that introduce an out-of-plane pin or fiber (e.g. stitching and z-pinning) affecting the overall microstructure, have also proven to enhance the composite fracture toughness [13–15].

In the literature, there are many studies investigating the cortical bone fracture toughening mechanisms and seeking possible applications on composite materials [16–23]. However, only few of them have manufactured bone-inspired composite materials and successfully implemented some of the characteristic bone toughening mechanisms into the synthetic counterparts [24–28]. Per contra, mimicking the fundamental toughening mechanisms has not always led to an enhancement in fracture toughness. For instance, in Libonati *et al* [26], mimicking the crack deflection mechanism did not yield an increase in fracture toughness, and limitations in the mechanical properties, measured in transversal direction, were also observed. Later on the authors showed some improvements in a new design though [24]. Recent improvements in additive manufacturing have enabled engineers to design and fabricate novel multifunctional composites with innovative properties [27,29–32]. However, the sought-after goal of fine-tuning the mechanical properties of composite materials put the needs for accurate and versatile numerical models to be embedded in the design phase. The main advantage of developing a numerical model of a composite material is the ability to adjust its parameters (i.e. topology and material properties) without the need of manufacturing and experimentally testing several samples. The development of numerical models is certainly time demanding. Yet, manufacturing different material topologies is not only equally challenging, but also harmful for the environment: a great deal of materials and energy must be wasted in the process.

Finite Element (FE) models represent the principal numerical approach to study the mechanics of composites [33]. In particular, different methods have been implemented into FE-codes with the aim of studying the fracture behavior and the mechanics of crack propagations. Commercial FE-based software allows the simulation of a crack, propagating in a structure subjected to any kind of loads, using two methods: Virtual Crack Closure Technique (VCCT) and Extended Finite Element Method (XFEM). The FEM (Finite Element Method) generally demands pre-processed mesh generation and involves mesh refinement in the area of particular interest (e.g. crack tip). Indeed, VCCT requires one to model the initial crack position and to use a finer mesh in the crack path. XFEM, instead, does not require remeshing in the crack tip region, being mesh independent [34–37]. Also, the crack position may or may not be pre-determined [37]. In the latter case, XFEM locates the possible crack initiation position by detecting the element, which corresponds to the critical state, indicated by chosen damage initiation [34]. XFEM, initially developed by Blytschko and Black [35], and recently implemented into commercial FE-codes, employs local enrichment zones in the crack tip, simulating the discontinuities when the crack opens. The current literature presents the application of XFEM in a broad number of fields, such as in biological tissues [16,17,38–40], bio-inspired composites [18], bonded joints [36], fiber reinforced composites [41–45], concrete [43,46,47] and laminated glass [48]. Duarte *et al* applied the XFEM to rubberized concrete [46] and, more recently, to fiber-reinforced composites [41], showing that the method can accurately estimate both the crack initiation and the propagation processes. Mishnaevsky and co-authors [49,50] implemented

XFEM into a multiscale framework to analyze fatigue-induced damage in hierarchical fiber-reinforced composites with different distribution of secondary nanoplatelet reinforcement. The versatility of the method and the freedom to set its parameters make XFEM an attractive approach to be implemented in various studies.

Here we adopted the XFEM implemented into a commercial finite element package, Abaqus 6.14 (Simulia, Providence, RI), to describe the mechanical behavior of a bio-inspired composite, whose design, manufacturing and characterization have been previously presented by Libonati *et al* [26]. We focused on the transversal behavior, which has shown to be the main limitation of the proposed design. The models, presented in the following, aim at simulating two loading conditions: tensile and flexural bending. The simulations are intended to provide a deeper understanding of the overall material behavior and its limitations, elucidating the effect of the microstructure and each topological feature, and providing the basis for an improved design. The simulations have also been used to probe the role of the cement line, a characteristic interface region with a crucial role in the fracture process of both the cortical bone and the bone-like composite. With the proposed model, the authors aim to deliver a tool able to elucidate the function of the bone microstructural features and their effect on the overall material properties, in particular the fracture toughness.

2. Computational model

2.1. Model geometry

The studied bioinspired design (**Figs. 1(b-c)**) implements the following bone features: i) the *osteons*, ii) the *cement lines*, iii) the *interstitial lamellae*, and iv) the *outer* *circumferential system*. The internal part of the osteons is reproduced by unidirectional bundles of glass fibers (UDGF) oriented longitudinally (along the z-axis), while the cement lines are reproduced by ±45° carbon fiber (CF) sleeves. The interstitial lamellae are made up of longitudinally-oriented UDGF bundles, which fill the gaps between the osteons. The outer circumferential system is replicated by means of two layers of UDGF non-crimp fabric (NCF), placed on both the top and the bottom of the arranged osteons. During the manufacturing process, the whole composite is impregnated by an epoxy resin. Hence, in the model we refer to the fiber-reinforced regions as UDGF/epoxy and CF/epoxy, according to the schematic shown in **Fig. 1(d)**. In the FE-models we introduced some simplifications with respect to the manufactured material. In particular, we considered the osteon cross section as perfectly circular; then, we considered the whole interstitial region as a mixture of UDGF and epoxy resin, without modeling the bundle shape. We believe that this is a more accurate representation of the manufactured composite, where the bundle cylindrical shape is lost during the manufacturing process, making the glass fibers completely interspersed into the matrix. This can be clearly noticed from the microscopic image provided in **Fig. 1(c)**. Further simplifications have been introduced to decrease the computational costs: when reproducing the tensile loading configuration, we modeled only a quarter of the repetitive unit cell, taking advantage of the symmetry of the topological structure (**Fig. A.1(a)**).

2.2. Numerical analyses and material properties

We carried out quasi-static simulations. All the analyses are based on the cohesive segment approach, which uses the traction-separation constitutive laws. The mechanical behavior is characterized by three regions: *i*) linear elastic, *ii*) damage initiation, and *iii*) damage evolution. The elastic properties define the initial tract, while damage initiation is set by the critical maximum principal stress criterion, similarly to other previous studies on fiber-composites [45,51]. Once the crack starts, the propagation and how the material cohesive stiffness degradation occurs are set by the damage evolution properties. To describe the damage evolution of each subregion, we adopted a displacement-based criterion. The material properties for each modeled region are given in **Table A.1** and **A.2**. Being this model a 2D representation of the transversal section, the UDGF/epoxy can be considered isotropic in-plane and the properties are provided by previous experimental tests carried out by the authors [52]. As critical stress for damage initiation (aka maximum principal stress, MAXPS, in Abaqus) of interstitial lamellae and outer circumferential system, we assumed the maximum stress experimentally determined by the authors in a previous study [26]. The failure mode observed in the experiments supports this assumption. For each region, the displacement at fracture was calculated using the characteristic length (*i.e.* 0.085 mm), which is the diagonal measurement of a rectangular element of 0.06 mm size. The models were built using four-node bilinear plain strain quadrilateral elements, with reduced integration and hourglass control (Abaqus element type CPE4R). A detailed description is given in the mesh convergence study, provided in the Appendix A.

To obtain the mechanical properties of the CF/epoxy that constituted the tubular sleeves aimed at mimicking the osteon cement lines, it was necessary to create a sub-model of the carbon fiber textile (**Fig. 2**). The dimensions of the fabric configuration (Twill 2x2) were acquired through measurements performed on microscopic images using the software

ImageJ 1.51K [53]. Then, the model was designed in the software TexGen 3.9 [54] under the following assumptions: *i*) the fiber fascicle course is sinusoidal, *ii*) the fascicle section has a lenticular shape, and *iii*) the average gap between the fascicles is not measurable, resulting in a tight configuration. The material properties for the carbon fibers and the resin regions were assigned, the model was exported to Abaqus and a mesh with eight-node brick elements with reduced integration (C3D8R) was applied. The boundary conditions were set, following the scheme provided by Li et al [55]. Two simulations were carried out with different mesh densities. Being the results were equivalent, the CF/epoxy properties were obtained (**Table A.2**) and used in the whole material model. The value of maximum principal stress, which defines the damage initiation of the CF/epoxy region, was obtained by the manufacturing supplier [56].

In the model aiming at simulating the tensile loading (**Fig. A.1a)**, the crack location was not assigned and all the regions were defined as enriched. The simulations were performed under displacement-control mode, where a positive displacement in x-direction was applied to the right-hand side. Other boundary conditions were: symmetry in both the left-hand side and the upper side. To overcome convergence issues, we increased the damage stabilization coefficient and the control parameters, allowing a discontinuous analysis to be performed.

For the three-point bending loading configuration (**Fig. A.1b)**, the simulations were also performed in displacement-control mode, reproducing the experimental setup. Non-specimen parts (*i.e.* loading member and rigid supports) were modeled as analytical rigid components. A displacement was applied to the loading member, while the rotation and displacement of the rigid supports were constrained in all directions. A surface contact between the specimen and the rigid members (*i.e.* loading and support) was set to occur in a tangential behavior, using a penalty formulation and a friction coefficient of 0.001. Except from the center region, the mesh was coarser: the element size was set to 0.2mm and a free mesh with advanced front technique was chosen. In the center region, we adopted a finer discretization: the element size was set to 0.06mm and a free mesh with respect to a medial axis was set. To improve the convergence, a 0.5mm flaw was also inserted in the lower extremity, as it appeared experimentally in the initial step of loading.

3. Results and discussion

The stress-strain curves and the failure modes of the two case studies are shown in **Fig. 3** and compared to the experimental outcome.

By comparing the results of the model under tensile loading, it can be seen that the failure mode approximates the experimental results: small initial cracks initiate in the interstitial lamellae, at the interface between the CF/epoxy and UDGF/epoxy regions; then another crack originates in the outer circumferential system (**Fig. 3(a)**), propagates through the interstitial region, and is finally deviated and arrested at the cement line (**Fig. 4(c)**). The inset in **Fig. 3(a)** shows the STATUSXFEM, which is a color-based representation of the status of the enriched elements (0.0 value indicates an uncracked element, whereas 1.0 value indicates a completely cracked element, with no traction across the crack faces). The model is also able to reproduce the stress-strain behavior of the experimental counterpart. Indeed, the numerical Young modulus is 11.9 GPa and failure occurred at a stress level of 29.8 MPa, values 18.3% lower and 6.4% higher than the experimental ones, respectively (**Figs. 4(a-b)**). It is fundamental to notice that there was no crack propagation through the cement line, as observed experimentally, confirming the fundamental role played by this interface region in the propagation of defects. The stress map (**Fig. 4(c)**) demonstrates the crucial role of the osteon shape in delocalizing the stresses, reducing the concentration at the crack tip, and the role of the cement line in deflecting and arresting the crack. The crack arrest caused a sudden drop in the load, which was considered as final rupture.

The results of the three-point bending loading condition are shown in **Fig. 3(b)** and **Figs. 4(d-f)**. The pre-modeled flaw propagates as the loading is applied and is temporarily arrested in the contact surface between the two adjacent osteons-like features. This partial arrest might also be caused by localized high aspect ratio elements, owing to the microstructure. After a small load drop, following the crack arrest, the crack keeps propagating until the final fracture point. The final failure occurs at the same displacement level of the experimental counterpart. However, the model shows a stress at rupture 21.7% higher than the one experimentally determined (**Fig. 4(d)**). The flexural modulus, calculated according to the standard (UNI-EN ISO 14125), is slightly lower (i.e. 8.6%) than the experimental one, as shown in the bar plot in **Fig. 4(e)**. Also in this loading condition, it is possible to notice the fundamental role played by the heterogeneous microstructure in altering the stress field, decreasing the stress concentration at the crack tip. Indeed, in this load case scenario, we can observe a stress concentration in the cement line, which might have prevented the crack propagation, influencing the path. The outcome of the simulations proves how the bone-like microstructure and some characteristic features (e.g. the cement line) can foster the activation of critical toughening mechanisms, increasing the overall flaw tolerance of the material and contributing to enhance the overall fracture toughness.

To provide a further understanding of the role of the cement line in the fracture behavior, we run two additional simulations. In these simulations, we neglected the cement line, modeling the osteon as a unique region. In the former, the osteon is modeled as CF/epoxy material, while in the latter as UDGF/epoxy. The results, shown in **Figs. 4(g-h)**, endorse the role played by the cement line. When the osteons are described as a unique CF/epoxy region, the failure mode is similar to the one presented in **Fig. 3(a)**, but the model has a lower toughness (*i.e.* 13%). Conversely, when the osteons are modeled as a unique UDGF/epoxy region, the damage occur simultaneously in the whole model, leading to a brittle failure and a lower toughness (*i.e.* 2%).

4. Concluding remarks

In summary, this paper presented a novel numerical approach, based on XFEM, to investigate the mechanical behavior of a de novo bio-inspired composite, previously designed, manufactured and tested by the authors, and the role of a characteristic microstructural feature (*i.e.* the cement line) in the fracture process. The outcome of this study shows that the models were able to mimic the experimentally observed behavior and toughening mechanisms, showing a good agreement in terms of mechanical properties and failure modes. Our results also shed light on the role of the cement line in our bone-inspired composite and demonstrate the importance of mimicking such feature - as interface region - in new bone-inspired materials, promoting the activation of characteristic toughening mechanisms and enhancing the fracture toughness. This proposed numerical approach can be used not only to predict the failure modes of composite materials, but also to investigate the role of the microstructure on the overall fracture behavior. The presented results may also provide a better understanding of the relationship between the structure and the properties in biological and biomimetic materials. Going forward, this framework could be used as a tool to improve the current design solution and propose future optimal solutions, also leveraging on optimization techniques.

Appendix A. Supplementary data

Supplementary data available: Schematics of loading and boundary conditions of the tensile model and the three-point bending model; Geometry and transversal properties of the regions; Properties of the CF/epoxy, epoxy resin and single carbon fiber; Convergence study, mesh of the tensile model and mesh of the central part of the three-point bending model.

Acknowledgements

The authors would like to acknowledge Francesco Ielmini for his help with Texgen.

Funding

This research did not receive any specific grant from funding agencies in the public, commercial, or not-for-profit sectors.

References

[1] Wegst UGK, Bai H, Saiz E, Tomsia AP, Ritchie RO. Bioinspired structural materials. Nat Mater 2015;14:23–36. doi:10.1038/nmat4089.

[2] Libonati F, Buehler MJ. Advanced Structural Materials by Bioinspiration. Adv Eng Mater 2017;19:1600787. doi:10.1002/adem.201600787.

[3] Pramanik A, Basak AK, Dong Y, Sarker PK, Uddin MS, Littlefair G, et al. Joining of carbon fibre reinforced polymer (CFRP) composites and aluminium alloys – A review. Compos Part Appl Sci Manuf 2017;101:1–29. doi:10.1016/j.compositesa.2017.06.007.

[4] Zabihi O, Ahmadi M, Nikafshar S, Chandrakumar Preyeswary K, Naebe M. A technical review on epoxy-clay nanocomposites: Structure, properties, and their applications in fiber reinforced composites. Compos Part B Eng 2018;135:1–24. doi:10.1016/j.compositesb.2017.09.066.
[5] Mittal G, Rhee KY, Mišković-Stanković V, Hui D. Reinforcements in multi-scale polymer composites: Processing, properties, and applications. Compos Part B Eng 2018;138:122–39. doi:10.1016/j.compositesb.2017.11.028.
[6] Barthelat F, Rabiei R. Toughness amplification in natural composites. J Mech Phys Solids 2011;59:829–40. doi:10.1016/j.jmps.2011.01.001.
[7] Launey ME, Buehler MJ, Ritchie RO. On the Mechanistic Origins of Toughness in Bone. Annu Rev Mater Res 2010;40:25–53. doi:10.1146/annurev-matsci-070909-104427.
[8] Koester KJ, Ager JW, Ritchie RO. The true toughness of human cortical bone measured with realistically short cracks. Nat Mater 2008;7:672–7. doi:10.1038/nmat2221.
[9] Nalla RK, Kruzic JJ, Kinney JH, Ritchie RO. Mechanistic aspects of fracture and R-curve behavior in human cortical bone. Biomaterials 2005;26:217–31. doi:10.1016/j.biomaterials.2004.02.017.
[10] Fantilli AP, Frigo B, Chiaia B. Comparing multi-scale cracking mechanisms in man-made composites and natural materials. Compos Part B Eng 2017;115:369–75. doi:10.1016/j.compositesb.2016.09.047.
[11] Guan J, Zhu W, Liu B, Yang K, Vollrath F, Xu J. Comparing the microstructure and mechanical properties of Bombyx mori and Antheraea pernyi cocoon composites. Acta Biomater 2017;47:60–70. doi:10.1016/j.actbio.2016.09.042.
[12] Bermejo R. “Toward seashells under stress”: Bioinspired concepts to design tough layered ceramic composites. J Eur Ceram Soc 2017;37:3823–39. doi:10.1016/j.jeurceramsoc.2017.04.041.
[13] Dransfield KA, Jain LK, Mai Y-W. On the effects of stitching in CFRPs—I. mode I delamination toughness. Compos Sci Technol 1998;58:815–27. doi:10.1016/S0266-3538(97)00229-7.
[14] Mouritz AP. Review of z-pinned composite laminates. Compos Part Appl Sci Manuf 2007;38:2383–97. doi:10.1016/j.compositesa.2007.08.016.
[15] Pingkarawat K, Mouritz AP. Comparative study of metal and composite z-pins for delamination fracture and fatigue strengthening of composites. Eng Fract Mech 2016;154:180–90. doi:10.1016/j.engfracmech.2016.01.003.
[16] Abdel-Wahab AA, Silberschmidt VV. Numerical modelling of impact fracture of cortical bone tissue using X-FEM. J Theor Appl Mech 2011;49:599–619.
[17] Abdel-Wahab AA, Maligno AR, Silberschmidt VV. Micro-scale modelling of bovine cortical bone fracture: Analysis of crack propagation and microstructure using X-FEM. Comput Mater Sci 2012;52:128–35. doi:10.1016/j.commatsci.2011.01.021.
[18] Baptista R, Almeida A, Infante V. Micro-crack propagation on a biomimetic bone like composite material studied with the extended finite element method. Procedia Struct Integr 2016;1:18–25. doi:10.1016/j.prostr.2016.02.004.
[19] Najafi AR, Arshi AR, Eslami MR, Fariborz S, Moeinzadeh M. Haversian cortical bone model with many radial microcracks: An elastic analytic solution. Med Eng Phys 2007;29:708–17. doi:10.1016/j.medengphy.2006.08.001.
[20] Huang J, Rapoff AJ, Haftka RT. Attracting cracks for arrestment in bone-like composites. Mater Des 2006;27:461–9. doi:10.1016/j.matdes.2004.11.022.
[21] Leuridan S, Goossens Q, Pastrav L, Roosen J, Mulier M, Denis K, et al. Determination of replicate composite bone material properties using modal analysis. J Mech Behav Biomed Mater 2017;66:12–8. doi:10.1016/j.jmbbm.2016.10.018.

[22] Libonati F, Vergani L. Understanding the structure–property relationship in cortical bone to design a biomimetic composite. Compos Struct 2016;139:188–98. doi:10.1016/j.compstruct.2015.12.003.

[23] Libonati F, Vergani L. Bone Toughness and Crack Propagation: An Experimental Study. Procedia Eng 2014;74:464–7. doi:10.1016/j.proeng.2014.06.298.

[24] Libonati F, Vergani L. Cortical Bone as a Biomimetic Model for the Design of New Composites. Procedia Struct Integr 2016;2:1319–26. doi:10.1016/j.prostr.2016.06.168.

[25] Libonati F. Bio-inspired Composites: Using Nature to Tackle Composite Limitations. In: Tiwari A, Murugan NA, Ahuja R, editors. Adv. Eng. Mater. Model., Hoboken, NJ, USA: John Wiley & Sons, Inc.; 2016, p. 165–90. doi:10.1002/9781119242567.ch5.

[26] Libonati F, Colombo C, Vergani L. Design and characterization of a biomimetic composite inspired to human bone. Fatigue Fract Eng Mater Struct 2014;37:772–81. doi:10.1111/ffe.12172.

[27] Libonati F, Gu GX, Qin Z, Vergani L, Buehler MJ. Bone-Inspired Materials by Design: Toughness Amplification Observed Using 3D Printing and Testing. Adv Eng Mater 2016;18:1354–63. doi:10.1002/adem.201600143.

[28] Naddeo F, Cappetti N, Naddeo A. Novel “load adaptive algorithm based” procedure for 3D printing of cancellous bone-inspired structures. Compos Part B Eng 2017;115:60–9. doi:10.1016/j.compositesb.2016.10.033.

[29] Gu GX, Takaffoli M, Buehler MJ. Hierarchically Enhanced Impact Resistance of Bioinspired Composites. Adv Mater 2017;29:1700060. doi:10.1002/adma.201700060.

[30] Dimas LS, Bratzel GH, Eylon I, Buehler MJ. Tough Composites Inspired by Mineralized Natural Materials: Computation, 3D printing, and Testing. Adv Funct Mater 2013;23:4629–38. doi:10.1002/adfm.201300215.

[31] Libonati F, Cipriano V, Vergani L, Buehler MJ. Computational Framework to Predict Failure and Performance of Bone-Inspired Materials. ACS Biomater Sci Eng 2017;3:3236–43. doi:10.1021/acsbiomaterials.7b00606.

[32] Gu GX, Libonati F, Wettermark SD, Buehler MJ. Printing nature: Unraveling the role of nacre’s mineral bridges. J Mech Behav Biomed Mater 2017;76:135–44. doi:10.1016/j.jmbbm.2017.05.007.

[33] Herakovich CT. Mechanics of composites: A historical review. Mech Res Commun 2012;41:1–20. doi:10.1016/j.mechrescom.2012.01.006.

[34] Goyal V, Irizarry E. Development of a Combined Cohesive and Extended Finite Element Method to Predict Delamination in Composite Structures. 57th AIAAASCEAHSASC Struct. Struct. Dyn. Mater. Conf., American Institute of Aeronautics and Astronautics; n.d. doi:10.2514/6.2016-0987.

[35] Belytschko T, Black T. Elastic crack growth in finite elements with minimal remeshing. Int J Numer Methods Eng 1999;45:601–20. doi:10.1002/(SICI)1097-0207(19990620)45:5<601::AID-NME598>3.0.CO;2-S.

[36] Stuparu F, Sandu M, Constantinescu DM, Apostol DA. A Combined Cohesive Elements—XFEM Approach for Analyzing Crack Propagation in Bonded Joints 2015. doi:10.1080/00218464.2015.1115355.

[37] Abaqus 6.14. Analysis User’s Manual 2014.

[38] Vergani L, Colombo C, Libonati F. Crack Propagation in Cortical Bone: A Numerical Study. Procedia Mater Sci 2014;3:1524–9. doi:10.1016/j.mspro.2014.06.246.

[39] Idkaidek A, Koric S, Jasiuk I. Fracture analysis of multi-osteon cortical bone using XFEM. Comput Mech 2017:1–14. doi:10.1007/s00466-017-1491-3.

[40] Budyn E, Hoc T, Jonvaux J. Fracture strength assessment and aging signs detection in human cortical bone using an X-FEM multiple scale approach. Comput Mech 2008;42:579–91. doi:10.1007/s00466-008-0283-1.
[41] Duarte APC, Díaz Sáez A, Silvestre N. Comparative study between XFEM and Hashin damage criterion applied to failure of composites. Thin-Walled Struct 2017;115:277–88. doi:10.1016/j.tws.2017.02.020.
[42] Bouhala L, Makradi A, Belouettar S, Kiefer-Kamal H, Fréres P. Modelling of failure in long fibres reinforced composites by X-FEM and cohesive zone model. Compos Part B Eng 2013;55:352–61. doi:10.1016/j.compositesb.2012.12.013.
[43] Benvenuti E, Orlando N, Ferretti D, Tralli A. A new 3D experimentally consistent XFEM to simulate delamination in FRP-reinforced concrete. Compos Part B Eng 2016;91:346–60. doi:10.1016/j.compositesb.2016.01.024.
[44] Ahmad H, Crocombe AD, Smith PA. Strength prediction in CFRP woven laminate bolted single-lap joints under quasi-static loading using XFEM. Compos Part Appl Sci Manuf 2014;66:82–93. doi:10.1016/j.compositesa.2014.07.013.
[45] Abdullah NA, Curiel-Sosa JL, Taylor ZA, Tafazzolimoghaddam B, Martinez Vicente JL, Zhang C. Transversal crack and delamination of laminates using XFEM. Compos Struct 2017;173:78–85. doi:10.1016/j.compstruct.2017.04.011.
[46] Duarte APC, Silva BA, Silvestre N, de Brito J, Júlio E. Mechanical characterization of rubberized concrete using an image-processing/XFEM coupled procedure. Compos Part B Eng 2015;78:214–26. doi:10.1016/j.compositesb.2015.03.082.
[47] Mougaard JF, Poulsen PN, Nielsen LO. Modelling concrete structures applying XFEM with a mixed mode constitutive model. Fract Mech Concr Concr Struct 2010;1:614–9.
[48] Chen S, Zang M, Wang D, Yoshimura S, Yamada T. Numerical analysis of impact failure of automotive laminated glass: A review. Compos Part B Eng 2017;122:47–60. doi:10.1016/j.compositesb.2017.04.007.
[49] Mishnaevsky L. Nanostructured interfaces for enhancing mechanical properties of composites: Computational micromechanical studies. Compos Part B Eng 2015;68:75–84. doi:10.1016/j.compositesb.2014.08.029.
[50] Dai G, Mishnaevsky L. Fatigue of multiscale composites with secondary nanoplatelet reinforcement: 3D computational analysis. Compos Sci Technol 2014;91:71–81. doi:10.1016/j.compscitech.2013.11.024.
[51] Arbabi N, Anbardan SAM, Hassanifard S. Finite element analysis of failure mechanisms in HDPE/$CaCo_3$ particulate composite. Plast Rubber Compos 2014;43:271–7. doi:10.1179/1743289814Y.0000000098.
[52] Libonati F, Vergani L. Damage assessment of composite materials by means of thermographic analyses. Compos Part B Eng 2013;50:82–90. doi:10.1016/j.compositesb.2013.01.012.
[53] Schneider CA, Rasband WS, Eliceiri KW. NIH Image to ImageJ: 25 years of image analysis. Nat Methods 2012;9:671–5.
[54] Brown, Louise P, Sherburn, Martin. TexGen V3.9.0. Zenodo n.d.
[55] Li S, Wongsto A. Unit cells for micromechanical analyses of particle-reinforced composites. Mech Mater 2004;36:543–72. doi:10.1016/S0167-6636(03)00062-0.
[56] ACP Composites. Mechanical Properties of Carbon Fiber Composite Materials 2014.

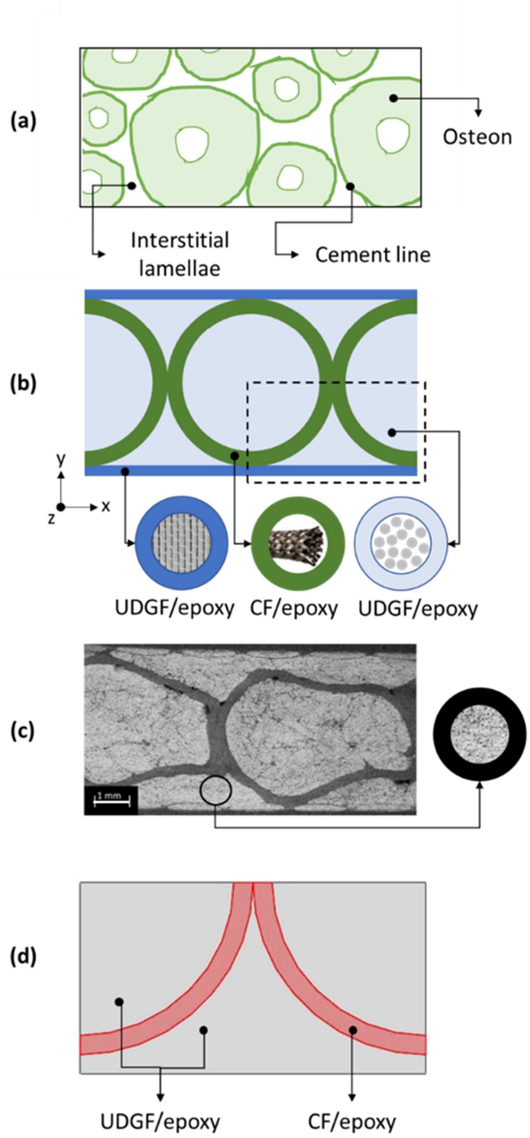

Fig. 1. (a) Schematic representation of the microstructure of cortical bone. (b) Schematic of the bioinspired design; the dashed area represents the repetitive unit. (c) SEM image showing the cross section of the previously developed bioinspired composite; scale bar 1mm. (d) Schematic of the modeled repetitive unit, highlighting the different subregions.

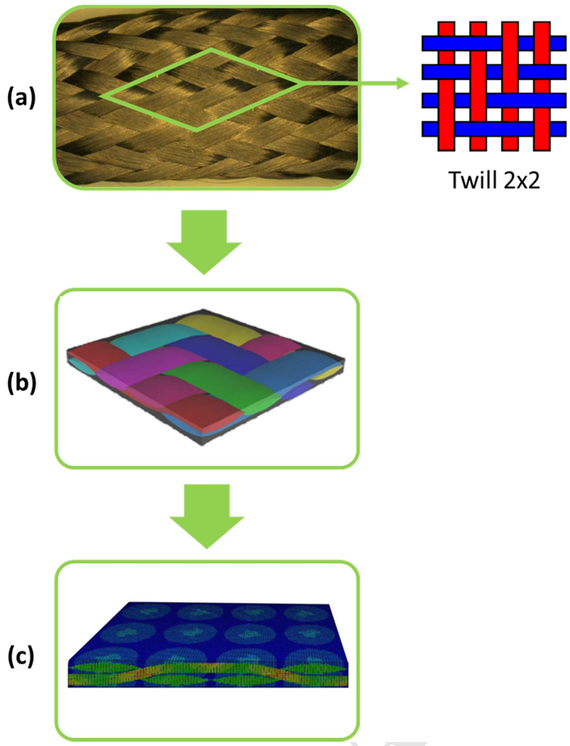

Fig. 2. Flow chart showing the steps followed to obtain the material properties of the CF-epoxy region. (a) Observation of the CF-sleeve by optical microscope and measurement of the yarn dimensions; highlighted the region of interest and, as magnification, a schematic of the fabric configuration (Twill 2x2). (b) Building of the unit cell model (geometry and mesh) in Texgen. (c) Simulations carried out on the unit cell to obtain the mechanical properties of the CF/epoxy region.

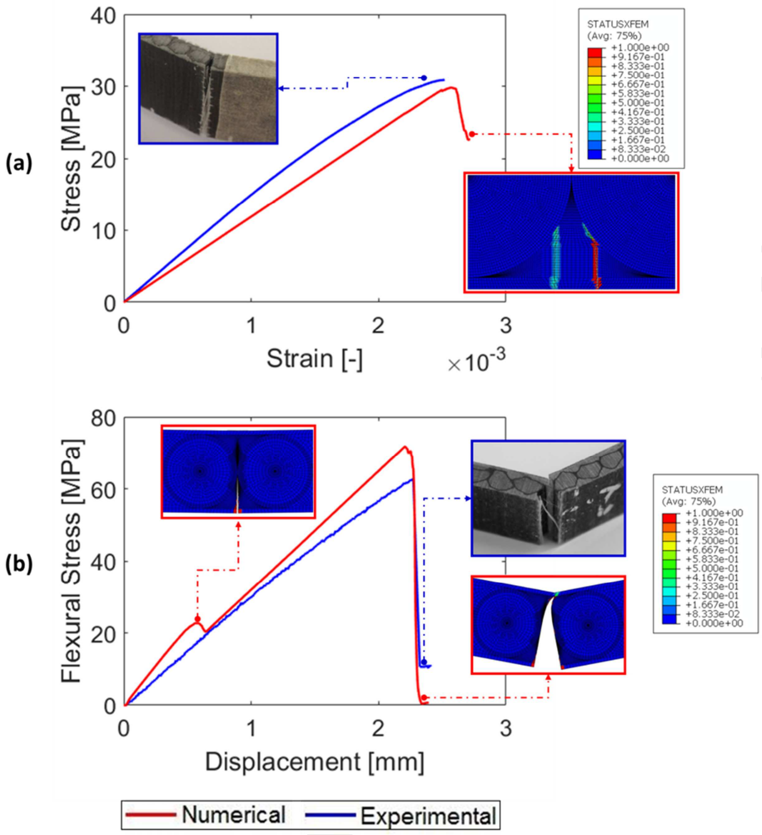

Fig. 3. Comparison between the experimental and the numerical results, in terms of mechanical performance, for the tensile (a) and the three-point bending tests (b), including the detailed fracture behavior. The insets representing the numerical fracture modes show the XFEM status, which is the status of XFEM elements (0.0 value indicates an uncracked element, whereas 1.0 value indicates a completely cracked element, with no traction across the crack faces). The b/w picture in inset (b), depicting the experimental failure mode under three-point bending loading is reproduced with permission from Fatigue & Fracture of Engineering Materials & Structures, Wiley-VHC ©2014 [26].

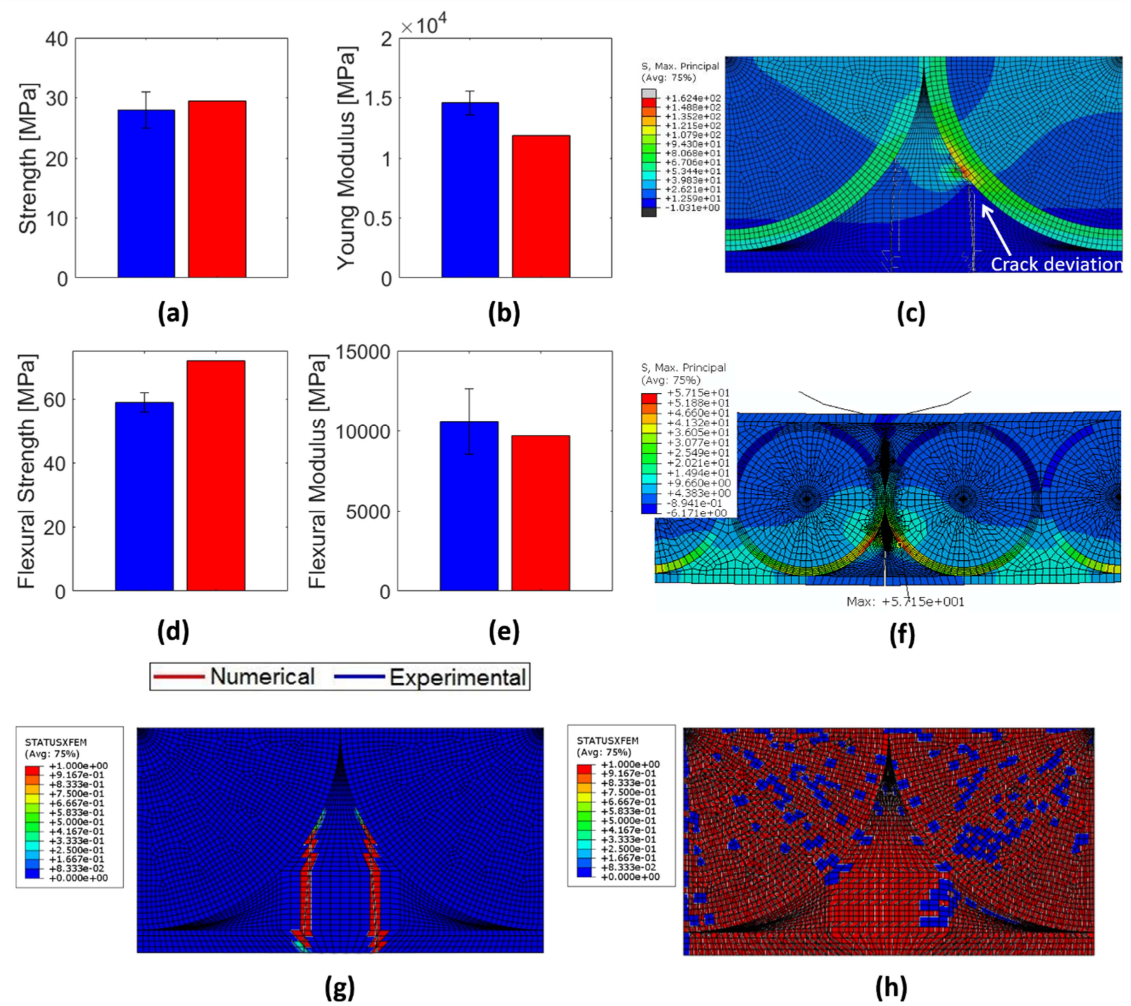

Fig. 4. Bar plots showing a comparison between numerical and experimental results for the tensile case study (a)-(b) and for the three-point bending one (d)-(e). (c) Visualization of the maximum principal stress distribution on the tensile model during failure. (f) Visualization of the maximum principal stress distribution on the flexural model during failure. The stress distribution demonstrates the crucial role of the osteon shapes in delocalizing the stresses, reducing the concentration at the crack tip, and the cement line in deflecting the crack. Failure mode when the osteon is modeled as a unique CF/epoxy region (g) or UDGF/epoxy region (h), neglecting the cement line.